

PAPER • OPEN ACCESS

Ion acceleration with few-cycle relativistic laser pulses from foil targets







To cite this article: Sargis Ter-Avetisyan *et al* 2023 *Plasma Phys. Control. Fusion* **65** 085012

View the [article online](#) for updates and enhancements.

You may also like

- [TESS Science Processing Operations Center FFI Target List Products](#)
Douglas A. Caldwell, Peter Tenenbaum, Joseph D. Twicken et al.
- [Atomic processes leading to asymmetric divertor detachment in KSTAR L-mode plasmas](#)
Jae Sun Park, Mathias Groth, Richard Pitts et al.
- [Final Targeting Strategy for the Sloan Digital Sky Survey IV Apache Point Observatory Galactic Evolution Experiment 2 North Survey](#)
Rachael L. Beaton, Ryan J. Oelkers, Christian R. Hayes et al.

Ion acceleration with few-cycle relativistic laser pulses from foil targets

Sargis Ter-Avetisyan^{1,*} , Parvin Varmazyar¹, Prashant K Singh¹, Joon-Gon Son¹, Miklos Fule¹, Valery Yu Bychenkov^{2,3} , Balazs Farkas⁴, Kwinten Nelissen⁴, Sudipta Mondal⁴ , Daniel Papp⁴ , Adam Börzsönyi⁴, Janos Csontos⁴, Zsolt Léczi^{1,4} , Tamas Somoskői⁴, Laszlo Tóth⁴, Szabolcs Tóth⁴ , Velyhan Andriy⁵, Daniele Margarone⁵, Ales Necas⁶, Gerard Mourou⁷, Gabor Szabó^{4,8} and Karoly Osvay^{1,8}

¹ National Laser-Initiated Transmutation Laboratory, University of Szeged, 6720 Szeged, Hungary

² P. N. Lebedev Physics Institute, Russian Academy of Sciences, 119991 Moscow, Russia

³ Center for Fundamental and Applied Research, VNIIA, ROSATOM, 127055 Moscow, Russia

⁴ ELI-ALPS, ELI-HU Non-Profit Ltd, Szeged, Hungary

⁵ ELI-Beamlines Facility, The Extreme Light Infrastructure ERIC, 252 41 Dolní Břežany, Czech Republic

⁶ TAE Technologies Ltd, Pauling, Foothill Ranch, CA, United States of America

⁷ IZEST, Ecole Polytechnique, Palaiseau, France

⁸ Department Optics and Quantum Electronics, University of Szeged, 6720 Szeged, Hungary

E-mail: ter-avetisyan.sargis@gmf.u-szeged.hu

Received 6 January 2023, revised 12 April 2023

Accepted for publication 13 June 2023

Published 3 July 2023



Abstract

Ion acceleration resulting from the interaction of 11 fs laser pulses of ~ 35 mJ energy with ultrahigh contrast ($< 10^{-10}$) and 10^{19} W cm $^{-2}$ peak intensity with foil targets made of various materials and thicknesses at normal (0°) and 45° laser incidence is investigated. The maximum energy of the protons reached ~ 1.4 MeV accelerated in the laser propagation direction and ~ 1.2 MeV in the opposite direction from a formvar target. The energy conversion efficiency from the laser to the proton beam is estimated to be as high as $\sim 1.4\%$ at 45° laser incidence using a 51 nm thick Al target. The high laser contrast indicates the predominance of vacuum heating via Brunel's effect as an absorption mechanism involving a tiny pre-plasma at the target front. The experimental results are in reasonable agreement with theoretical estimates, where proton acceleration from the target front side in the backward direction is well explained by the Coulomb explosion of a charged cavity formed in a tiny pre-plasma, while forward proton acceleration is likely to be a two-step process: protons are first accelerated in the target front-side cavity and then further boosted in energy through the target back side via the target normal sheath acceleration (TNSA) mechanism.

Keywords: laser plasma ion acceleration, few-cycle laser interaction with matters, laser plasma ion acceleration scenarios

(Some figures may appear in colour only in the online journal)

* Author to whom any correspondence should be addressed.



Original content from this work may be used under the terms of the [Creative Commons Attribution 4.0 licence](https://creativecommons.org/licenses/by/4.0/). Any further distribution of this work must maintain attribution to the author(s) and the title of the work, journal citation and DOI.

1. Introduction

At the dawn of the field, it was possible to accelerate protons and ions above MeV energies with large-scale laser systems firing only a few times an hour. So far, the highest laser-to-ion conversion efficiency has been demonstrated with sub-ps laser pulses [1]. Laser systems with pulse durations of a few tens of femtoseconds provide the necessary peak intensity, but with a lower pulse energy and a higher repetition rate [2]. Various experiments [3–7] and theoretical studies [8–13] have investigated the acceleration mechanisms on thin targets and optimised the ion yield. Such laser-driven ion beams have demonstrated their credibility for applications in a wide range of areas, e.g. probing of fields in plasmas [14], generation of directional neutron sources [15], isochoric heating of solid matter [16], and radiobiology [17, 18]. Recent developments in sub-50 fs laser systems have made it possible to optimise ion acceleration [19, 20] and start building beamlines dedicated in particular to the medical use of laser-accelerated ions [21–23].

The advances in laser technology have led to the generation of laser pulses with durations of only a few optical cycles. Due to the very short pulse duration as well as the extreme beam quality, it has become possible to reach relativistic intensity in the focus with a few tens of mJ pulse energy. At such low energy, few-cycle laser systems are capable of operating at kHz repetition rate over 24/7 with high reliability [24]. This is accompanied by the development of kHz repetition rate target systems, such as gas jets [25] and thin liquid leaves [26], offering an opportunity to generate stable electron [27] and ion beams [28] and, possibly, gamma rays. These could be highly beneficial for medicine, industry, science, and homeland security [29]. For example, high repetition rate ion sources can serve as input beams for diverse accelerator systems, meeting the requirements of high current, low and high charge state, and low emittance [30]. Deuterons accelerated to energies above 0.5 MeV at kHz repetition rate can generate a large flux of neutrons per second via a $D(d,n)$ reaction. Radioisotope production with kHz repetition rate is another potential application for nuclear pharmacology [31, 32]. Apart from an early work [33] and a recent study [34] with somewhat lower intensity on a bulk target, experimental results on ion acceleration with few-cycle relativistic pulses are yet to be disseminated.

In this paper, we discuss our recent experimental findings with the use of ultrahigh contrast, few-cycle laser pulses of relativistic intensity on diverse target materials, thicknesses, and angles of incidence. The measurements show new features in the ion acceleration scenario. The maximum energy for protons was measured to be just above 1 MeV, being far less affected by the target material (metal or dielectric) and thickness than expected from present ion acceleration theories [8–13]. At a laser incidence angle of 45° , the properties of proton emissions from the rear and the front of the target surface were similar. The cut-off energy was, however, about half of that at normal laser incidence on the target. We also provide

quantitative explanations for the novel features observed in the given ion acceleration scenario.

2. Experimental setup

In the experiments, the charged particles were generated by irradiating foil targets with the SYLOS Experimental Alignment (SEA) Laser at the ELI-ALPS facility in Szeged, Hungary [24]. In the experiments (figure 1(a)), p -polarised, 11 fs laser pulses of ~ 35 mJ energy were focused using an $f/2.5$ off-axis parabolic mirror. The power-weighted central wavelength of the broadband structured pulse spectrum is 846 nm. The spatial energy distribution of the laser pulse in the focal plane was measured by a 16-bit CCD camera with an optical magnification close to $50\times$ (figure 1(b)). The central spot with a size of $2.9 \mu\text{m} \times 3.5 \mu\text{m}$ (FWHM) contains 36% of the total energy. Hence, the peak intensity driving the interaction is $I \cong 10^{19} \text{ W cm}^{-2}$. It is worth mentioning that the measured ultrahigh contrast $< 10^{-10}$ (figure 1(c)) is still conservative due to the bandwidth limitation of the third-order cross-correlator (Sequoia by Amplitude Tech.). Since the standard thicknesses of the non-linear crystals support a bandwidth of half of the SEA laser pulse, the laser pulse peak intensity and, hence, the temporal contrast is underestimated. As a consequence, the contrast is expected to be approximately eight times higher than that shown in figure 1(c).

The foil targets of different materials, namely carbon (C), diamond-like-carbon (DLC), formvar ($[\text{CH}_2\text{CH}(\text{OH})]_n$), and aluminium (Al), were irradiated at incidence angles of 0° and 45° with respect to the target normal. The target thickness varied in the range of $5 \text{ nm} - 9 \mu\text{m}$. A target alignment system consisting of an infinity-corrected long working distance objective located along the axis of the incident laser beam was used to visualise the laser focal spot and position the target in the same focal spot. The targets were positioned with an accuracy of $5 \mu\text{m}$ at the laser focal plane [35], which ensured high reproducibility and reliability of the experimental data.

The ion spectra were measured in a single laser shot with a calibrated Thomson spectrometer [36] located along the rear or front surface target normal direction, later called the forwards (FWD) and backwards (BWD) directions, respectively. The collection of ions below a solid angle of 30 nsr ensured the measurement of well-resolved ion spectra within the energy range of the spectrometer $E_i/Z \approx 0.025 \div 2 \text{ MeV/nucleon}$. Typically, a magnetic field of $(0.27 \pm 0.01) \text{ T}$ and an electric field of up to 3 kV cm^{-1} were applied. The energy resolution of the spectrometer at high energies (above 0.5 MeV) was $\Delta E/E_i \sim 5\%$. The ions were detected by a multichannel plate (MCP) detector coupled to a phosphor screen. Our particular interest is the ion spectrum, from which the maximum ion energy as well as the number of ions can be obtained. Typical measured ion spectral traces are shown in figure 2, along with the corresponding evaluated proton spectrum.

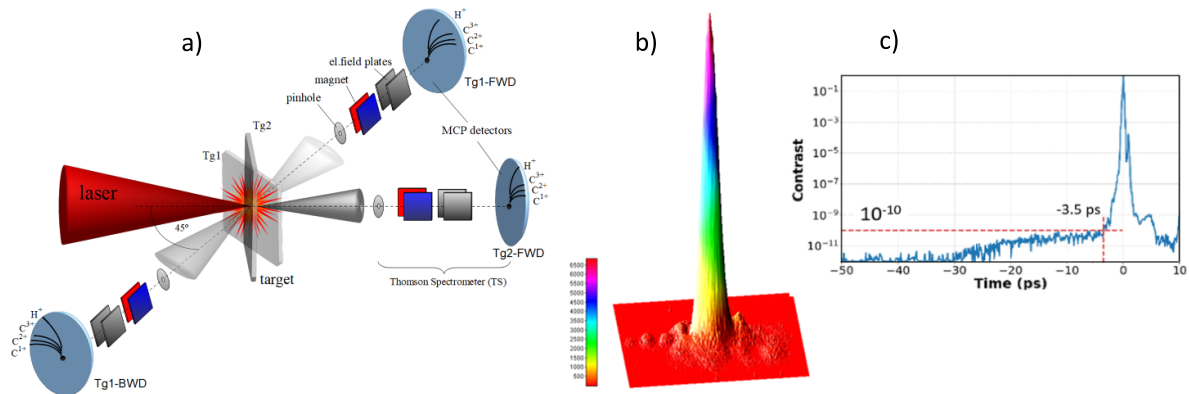


Figure 1. (a) Schematic of the experiment. Laser incidence angle on targets Tg1 and Tg2 is 45° and 0° , with respect to target normal, respectively. The Thomson spectrometers located along the target normal directions measured the ions from Tg1 in Tg1-FWD and Tg1-BWD directions, and from Tg2 in Tg2-FWD direction. (b) The laser pulse intensity distribution (in arbitrary units) in focal plane, measured with a magnification $50\times$ has a size $2.9\ \mu\text{m} \times 3.5\ \mu\text{m}$ (FWHM). (c) The measured temporal contrast of the laser pulse.

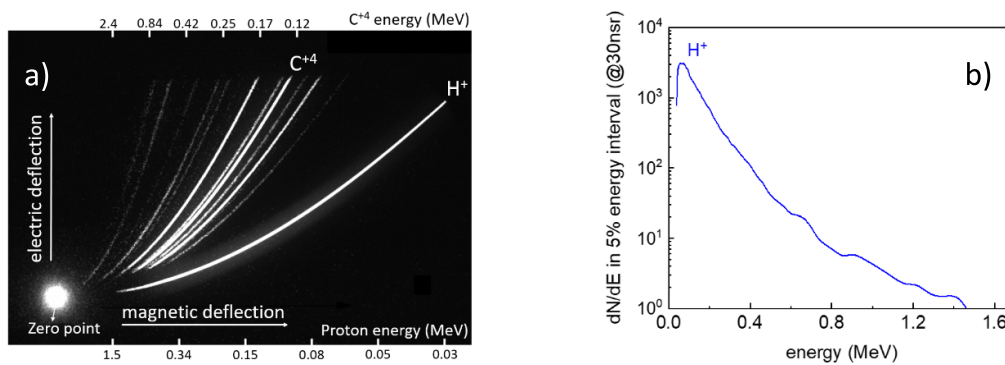


Figure 2. (a) A typical CCD picture of measured ion spectra from a 26 nm formvar target, as an example, and (b) the evaluated proton spectrum (the background is subtracted).

3. Experimental results

At an incidence angle of 45° on the target, the maximum proton energies observed in the FWD and BWD directions versus the target thickness and materials are shown in figures 3(a) and (b), respectively. Protons with the highest cut-off energy of around 1.4 MeV are accelerated from 26 nm and 660 nm thick formvar targets. Another noticeable feature here is that the acquired maximum energy of protons from the other targets with thicknesses from $2\ \mu\text{m}$ down to 20 nm weakly depends on the target thickness. In FWD (figure 3(a)), the measured maximum proton energy (1.2 ± 0.3 MeV) is found to be around 200 nm, slightly decreasing to about 0.8 MeV for the thinnest (5 nm) and the thickest ($9\ \mu\text{m}$) targets. In BWD (figure 3(b)), the proton energies are somewhat lower (compared to that in FWD); nevertheless, in both cases, the formvar targets show a higher proton cut-off energy compared to other target materials. In FWD, the proton energy from the formvar target is only about 1.2 times higher than in BWD, while for the other target materials the difference is almost twice. It is worth mentioning that symmetric proton emission in the FWD and BWD directions was also observed in [37] with a peak intensity similar to ours. However, their pulse duration and energy were ~ 6 times longer and ~ 18 times higher than those of

our experiment, being very far from the few-cycle regime. In a few-cycle regime of ultrahigh clean pulse the asymmetric behaviour we observed suggests some peculiar features of proton acceleration. The implications on the acceleration conditions, including pre-plasma effects on the front and back of the target, are discussed in a further chapter of this paper.

In figures 3(c) and (d), the number of protons emitted in a 30 nsr solid angle along the FWD and BWD directions is shown. The number of particles is integrated above 100 keV up to the cut-off energy. It is worth noting that it is not always the spectrum with the highest cut-off energy that shows the highest particle yield. In figures 3(c) and (d) the measured highest proton yield is about 10^5 protons within a factor of 2–4, while the target thickness varies by several orders of magnitude.

At a 0° angle laser incidence on the target, the maximum proton energies versus the target thickness observed in the FWD direction are shown in figure 4(a) for different foil materials. Here, compared to a 45° laser incidence (figure 3), the energies are over a factor of two lower, while the integrated number of protons is an order of magnitude lower. The exception is the formvar target, where the integrated number of protons is about the same as at 45° laser incidence. However, it shows a similar dependence of the cut-off energy to 45° laser incidence, with a slight decrease at the thinnest and the thickest

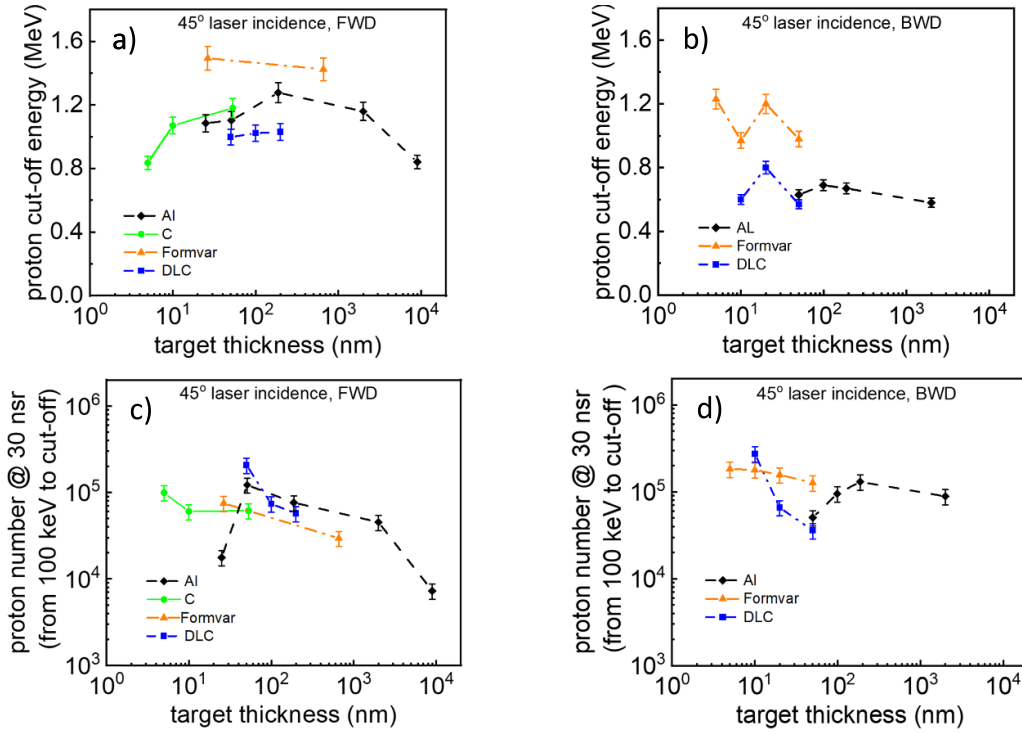


Figure 3. (a), (b) The maximum energy of protons and (c), (d) highest number of protons versus thickness of the target emitted in FWD (a), (c) and BWD (b), (d) directions are shown at 45° laser incidence angle on different target materials.

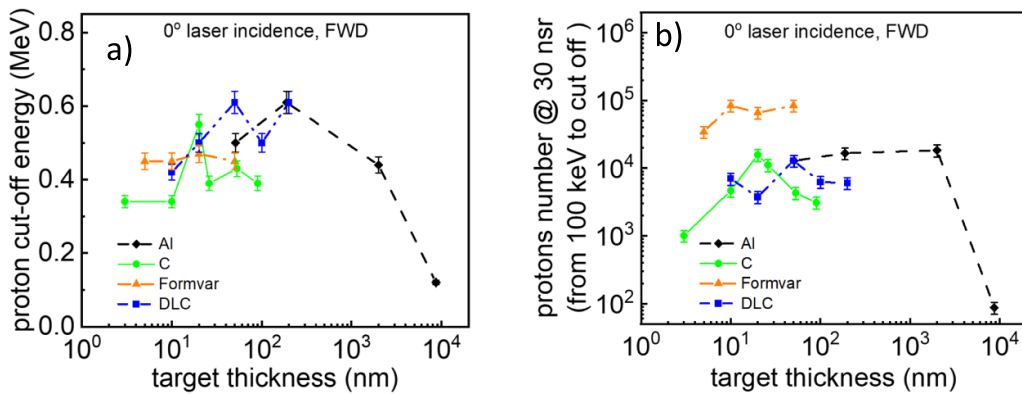


Figure 4. (a) The maximum energy of protons and (b) the highest number of protons versus thickness emitted by the target in FWD direction are shown at 0° laser incidence angle on the target for different target materials.

targets and a similar tendency to be almost independent of the target material. Such a weak dependence of the proton cut-off energy on the target thickness may indicate that under our conditions, the electron transport and electron dynamics inside the target do not play a significant role in the ion acceleration process. This suggests that the dominant role in ion acceleration is played by processes at the target front, where the laser energy is transferred to hot electrons in a similar way for all the investigated target thicknesses.

Figure 5 shows the emitted ion spectra in FWD for five successively increased thicknesses of Al target at the same laser irradiance and at a 45° laser incidence angle on the target. An interesting phenomenon is that the carbon ions are mostly observed for the thinnest targets with a dominance of C⁴⁺. The ion charge-state density gradually decreases when

the target thickness is increased, while the maximum energy of ions remains virtually unchanged. For thicker targets, the number of carbon ions drops well below the detection limit (limited by the solid angle of reception of the Thomson spectrometer) and only protons are detected. This may be due to the scattering of ions accelerated from the charged cavity as they propagate through the target: the thicker the target, the more the ions scatter.

In the spectra of BWD accelerated ions, this phenomenon was not observed. Carbon ions with a dominance of C⁴⁺ were present in all cases. At a 0° laser incidence angle, it is difficult to make a clear statement since at this geometry, the particle number dropped by about an order of magnitude. Hence, the changes we see could be related to the low number of detected particles.

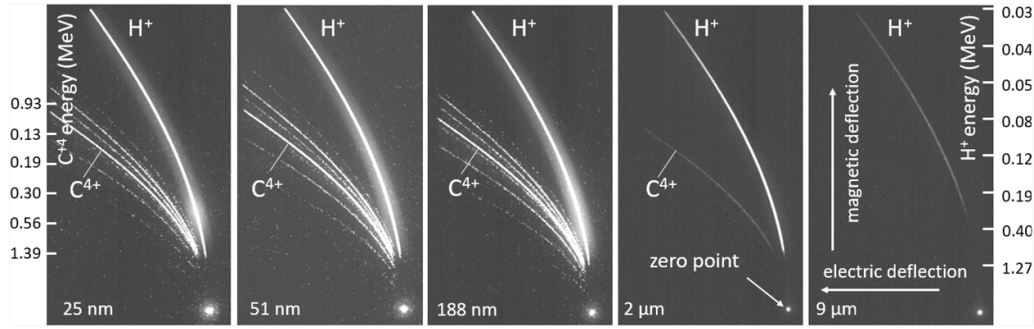


Figure 5. The emitted ion spectral parabolic traces from Al target measured in the FWD direction at four successively increasing thicknesses with the highest proton cut-off energy.

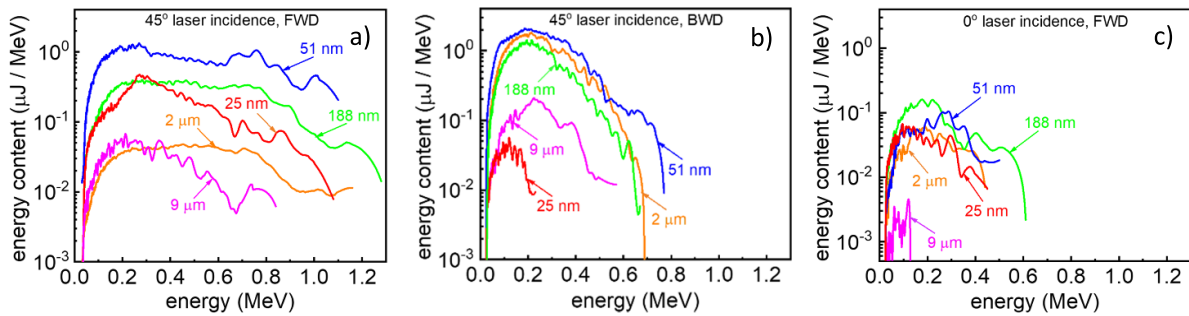


Figure 6. The spectral energy content in the proton beam from Al targets at different thicknesses for FWB and BWD directions at 45° laser incidence and for FWD at 0° incidence.

4. Conversion efficiency

From the measured number of particles in the ion spectra (figures 3(b), (d), and 4(b)) and the measured divergence of the proton beam of 5° (see [38]), one can derive the spectral energy content in the proton beam. The assumption that the divergence of the proton beam is the same for all target thicknesses is rather conservative as the proton beam divergence may increase as the target thickness decreases. The figure 6 shows the spectral energy content in the proton beam for an Al target, the one with the most systematic change of target thickness, both in FWD and BWD directions at 45° (figures 6(a) and (b)), and in FWD direction at 0° angle of incidence (figure 6(c)). It is noteworthy that at 45° laser incidence in the FWD direction (figure 6(a)) there is a plateau in the energy content in the beam with energies of 0.2 MeV–0.8 MeV for 51 nm, 188 nm, and 2 μm thick targets. For the thinnest (25 nm) and the thickest (9 μm) targets there is a clear maximum at around 0.2 MeV. The plateau was not observed in BWD at 45° (figure 6(b)) nor FWD at 0° laser incidence (figure 6(c)). Instead, the energy content in the beam had a maximum of about 0.2 MeV for all thicknesses besides the 9 μm target, where the energy content was an order of magnitude lower (figures 6(b) and (c)).

On the whole, all this indicates a highly efficient transfer of laser energy to the target and acceleration of ions. On the basis of the energy content of the beam shown in figure 6, a conservative estimate can be given for the conversion efficiency of laser energy to protons. Figure 7 shows the conversion efficiency of laser energy into protons with energies above

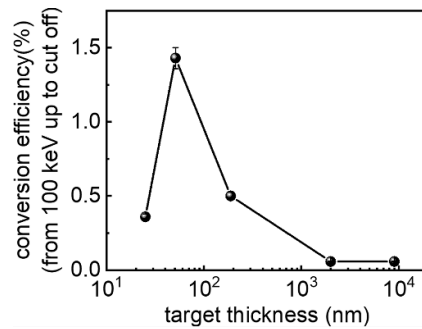


Figure 7. Dependence of the conversion efficiency of laser energy into protons with energies above 100 keV on the thickness of Al targets in FWD direction at a 45° laser incidence angle (derived from figure 6).

100 keV to the cut-off for Al targets, depending on the target thicknesses. Here, we assumed that the divergence of the proton beams is independent of the proton energy within the measured energy range, in agreement with [39, 40]. There is a clear maximum, reaching ~1.4% at a 51 nm thick target. However, the optimum target thickness can be given with some uncertainty due to the target thickness steps.

It is known that the target thickness, L , should be properly matched to the laser intensity distribution, which includes both the peak intensity and pre-pulse level, in order to obtain the maximum ion energy. Earlier numerical models showed that protons can be accelerated to the highest energies at the targets of optimum thickness and density [9–11, 13] with a clear trend of increasing ion energy with decreasing target thickness

to the nanoscale. This has also been proven by experiments with multi-Joule, very high contrast laser pulses [41, 42]. For target thicknesses at which relativistic self-induced transparency occurs near the laser peak [43], the protons acquire a high energy. In the experiments, the target thickness and laser pre-pulse were found to be key factors for the high conversion efficiency of $\sim 4\%$ at $10^{21} \text{ W cm}^{-2}$ [6], or, for optimisation of the source properties [3]. Hence, the proper selection of foil target optimum thickness for certain laser parameters results in a very promising increase in the proton energy. We emphasise that a scale length of pre-plasma, which appears due to the finite laser intensity contrast ratio (figure 1(c)), enhances the laser energy absorption and particle acceleration [42, 44, 45] unless, of course, it destroys a thin target. It is worth noting that even in the case of ‘ideal’ contrast, there is a pre-pulse of natural origin associated with the temporal profile of the laser pulse, e.g. with a Gaussian pulse profile, so the pre-plasma expansion starts at the rising edge of the pulse from already $I_0 \sim 10^{10} \text{ W cm}^{-2}$ at about 30 fs before the maximum intensity is reached on the target. It determines the appropriate target thickness for the most efficient acceleration.

In accordance with figure 1(b), plasma production at the front of the Al target, which requires an intensity of $I_0 \gtrsim 10^{10} \text{ W cm}^{-2}$, takes place at $t > t_0 \sim -(3-2)$ ps before the maximum laser intensity arrives at the target. With an expansion velocity of $c_s \sim (1-2) \times 10^4 \text{ m s}^{-1}$ [46], a pre-plasma with a characteristic scale length of $L_{pp} = c_s t_0 \sim 30 \text{ nm}$ in the form of a density ramp, $\propto \exp(x/L_{pp})$, appears in front of the target. It consists of a mixture of Al and hydrocarbon contaminant ions naturally present in the $\sim 3 \text{ nm}$ layer [47].

If the target thickness $L < L_{pp}$, then the target evaporates before the femtosecond laser pulse arrives. Therefore, for an Al target with thickness $L \lesssim 30 \text{ nm}$, the efficiency of ion acceleration is expected to decrease drastically as we see in figure 7, where destruction of the foil likely takes place for targets thinner than the 50 nm optimal thickness. For dielectrics, the threshold of plasma production is an order of magnitude higher ($I_0 \sim 10^{11} \text{ W cm}^{-2}$) and $t_0 \sim 1 \text{ ps}$, which makes it possible to use even thinner foil, up to $L \lesssim 10 \text{ nm}$, as in the case of the formvar target (see figure 4). In this respect, our results are in agreement with those obtained in [42], where for a laser pulse intensity of $\sim 10^{21} \text{ W cm}^{-2}$ at 1J, the proton energy still increased as the dielectric target thickness decreased to 30 nm when the laser pre-pulse was removed prior $t_0 \sim -1 \text{ ps}$.

5. Discussion

5.1. 45° laser incidence on the target

During the incidence of ultrashort and ultrahigh-contrast laser pulses on a target with a step-like density profile, the laser energy is transferred to the electrons mainly due to the so-called vacuum heating via the Brunel effect [48, 49] and $v \times B$ heating [50]. For a moderately relativistic pulse (with a standard dimensionless laser field amplitude, $eE_{L0}/m\omega_{L0}c = a_0 \sim 2$, where E_{L0} , ω_{L0} are the laser field and laser field frequency,

and e , m are the electron charge, and mass, respectively) the Brunel effect dominates. This is consistent with the higher laser-to-ion energy conversion efficiency in our experiment (see figure 6) for the oblique rather than the normal incidence case (see also [34]). Even if the size of the density ramp at the target surface is smaller than the electron quivering amplitude under Brunel’s effect, such tiny pre-plasma as $L_{pp} \sim 30 \text{ nm}$ makes a considerable contribution to electron heating/acceleration in both the laser field (E_{L0}) and electrostatic field ($E_{el.st.}$), which determines the nature of the nonlinear Brunel effect [51]. Indeed, effective electron acceleration/heating forms a well-pronounced electron cloud around the thin target with dominance in the FWD direction. Hence, formed charge separation field most effectively accelerates ions from the target rear in the FWD direction that is called target normal sheath acceleration (TNSA) mechanism. We consider it as the source of FWD accelerated protons in our experiment.

5.1.1. BWD accelerated ions. We consider the acceleration mechanism proposed in [52] to explain experimental findings at the interaction of a relativistic intense laser pulse with a solid target with a step-like density profile. This is attributed to the formation of a positively charged cavity in the form of a pancake at the target front via the laser light pressure pushing electrons out. The thickness of this cavity is given by the balance of the Coulomb force and the light pressure force, $E_{L0} = E_{el.st.}$, which determines the Coulomb explosion of the cavity and acceleration of protons. The mechanism was recently applied to a tiny pre-plasma at a solid target surface, where a charged cavity is formed in the domain of laser light reflection [34].

We estimate the maximum energy of BWD accelerated protons, ε_m , from the exploding cavity, as the work done by the cavity Coulomb field to move protons out of the cavity,

$$\varepsilon_m \simeq eE_{el.st.} l_{acc}, \quad (1)$$

where l_{acc} is the entire acceleration length and $E_{el.st.}$, in accordance with [53, 52], is estimated as E_{L0} . One can assume that the maximum possible acceleration length is $l_{acc} \simeq R$, where R is the laser focal spot radius, since at a distance longer than R , the accelerating Coulomb field drastically drops due to the transition from a 1D to a 3D geometry. However, for a too short laser pulse, the accelerating field disappears before ions reach the distance $\simeq R$, because the laser light pressure terminates at the end of the pulse, destroying the positively charged cavity. Correspondingly, the acceleration length can be approximated as $l_{acc} \simeq \langle v \rangle \tau \simeq (v_m/2) \tau$, where we assume the ions are initially at rest. Here, τ is the pulse duration and $\langle v \rangle$ is the characteristic velocity of the expanding ion front, which can be estimated as $v_m/2$, where $v_m = (2\varepsilon_m/M)^{1/2}$ and M is the mass of the proton.

Substitution of the value $l_{acc} \simeq \langle v \rangle \tau$ in equation (1) gives the proton acceleration length as

$$l_{acc} \simeq \frac{c}{\omega_{L0}} \frac{m}{M} (\omega_{L0} \tau)^2 \equiv l_i \quad (2)$$

which takes place in the case of short enough and/or rather weak laser pulses, i.e. under the following condition:

$$\omega_{L0}\tau < \sqrt{\frac{R\omega_{L0}}{c} \frac{M}{ma_0}}. \quad (3)$$

For this condition, the maximum proton energy equation (1) gained over the length equation (2) reads

$$\varepsilon_m \simeq mc^2(a_0\omega_{L0}\tau)^2 \frac{m}{M}, \quad (4)$$

while for the longer or/and stronger laser pulses, when opposite to equation (3) inequality holds, the cut-off energy reaches its maximum value:

$$\varepsilon_m \simeq mc^2 a_0 \frac{R\omega_{L0}}{c}. \quad (5)$$

Based on equations (4) and (5), a simple interpolation formula for the estimation of the maximum proton energy from the exploding laser created cavity can be proposed:

$$\varepsilon_m \simeq mc^2 a_0 \frac{\omega_{L0}}{c} \frac{l_i R}{l_i + R}, \quad (6)$$

This is an easy-to-use estimate for the arbitrary laser pulse duration. Here, $l_i(\tau)$ is given by equation (2).

As the laser field amplitude decreases with the pulse duration, $a_0 \propto 1/\sqrt{\tau}$, we conclude from equations (4)–(6) that for a given light energy fluence (Φ_0) there is an optimum pulse duration for which the cut-off energy is maximum, which is defined by the equality $l_i(\tau) \simeq 2R$, or in the explicit form

$$\omega_{L0}\tau \simeq \sqrt[3]{\frac{cR^2 M^2 \omega_{L0}^3}{2\pi e^2 \Phi_0}}. \quad (7)$$

Correspondingly, for a given laser pulse energy and duration, equations (4)–(6) make it possible to understand the optimal radius needed to reach the maximum cut-off energy ε_m . In this case, the tightest focus seems to be the most optimal. However, this is true only until the focusing reaches the diffraction limit, $2R \sim \lambda_0$, because in this limit it is likely that the complex multicomponent structure of the electromagnetic laser field will destroy the cavity. Finally, we note that for short laser pulses, when condition equation (3) holds, the laser-to-proton conversion efficiency is independent of the laser intensity, while for long pulses the square root dependence of ion energy equation (5) (see [52]) results in a square root decrease in the conversion efficiency, $\propto 1/\sqrt{I}$, with the laser intensity.

In our case of a very short laser pulse of moderate intensity, we are at the limit of applicability of equation (4). For $a_0 \simeq 2$ and $\tau \simeq 11$ fs, the maximum energy of the BWD accelerated protons is $\varepsilon_m \simeq 0.7$ MeV, which is in good agreement with measurements (figure 3(b)).

5.1.2. FWD accelerated protons. Naturally, the first mechanism to investigate is TNSA caused by laser-produced hot electrons. The TNSA mechanism [53] is widely considered as isothermal backside plasma expansion. However, for very short, few-cycle pulses, the effect of electron cooling must be taken into account. The cooling starts after the end of the laser pulse and reduces the acceleration efficiency. The TNSA mechanism should be applied to the standard situation of a two-component electron plasma consisting of laser-produced hot electrons and cold target electrons with effective energies ('temperatures') and densities, $T_{h \text{ or } c}$ and $n_{h \text{ or } c}$, correspondingly [54]. If the hot electrons dominate in the plasma energy density, $n_h T_h > n_c T_c$, the maximum proton energy during acceleration reads

$$\varepsilon_m \simeq T_h \left[\ln \left(\frac{t}{\tau_0} + \sqrt{\left(\frac{t}{\tau_0} \right)^2 + 1} \right) \right]^2, \quad (8)$$

where $\tau_0 = \lambda_{Dh}/c_p$, $c_p = \sqrt{T_h/M}$, and λ_{Dh} is the Debye length of hot electrons. In equation (8) it is assumed that the hot electron temperature does not change, which is, strictly speaking, only true during the laser pulse. On the other hand, after the pulse terminates, the temperature of hot electrons drops over time as $\propto 1/(1+t^2/\tau_0^2)$, i.e. proton acceleration lasts for τ_0 after the end of the laser pulse.

Thus, taking into account that the energy gain by the proton lasts $\simeq \tau + \tau_0$, equation (8) is transformed to

$$\varepsilon_m \simeq T_h \left[\ln \left(1 + \frac{\tau}{\tau_0} + \sqrt{\left(1 + \frac{\tau}{\tau_0} \right)^2 + 1} \right) \right]^2, \quad (9)$$

i.e. as a function of the pulse duration, the ion energy cut-off demonstrates a $\ln^2 \tau$ increase. However, for long pulses, almost regardless of the further increase in τ , the ion energy approaches the maximum possible cut-off energy: $\varepsilon_m \simeq T_h \ln^2(2R/\lambda_{Dh})$ since even at very long laser pulses the effective acceleration length is limited by the size of the focal spot radius.

To estimate the cut-off energy using equation (9), knowledge of hot electron characteristics (T_h , n_h) is required. On this path, we will follow a simple, often used approach. We apply the ponderomotive estimate for $T_h = mc^2(\sqrt{1+a_0^2/2}-1) \approx 370$ keV [36] and estimate n_h from the energy flux balance $T_h n_h v_h = \eta I_0$, where η is the laser energy absorption coefficient and v_h is the characteristic electron velocity (close to the speed of light), $v_h = c(\varepsilon^2 + 2\varepsilon)^{1/2}/(\varepsilon + 1)$, $\varepsilon = T_h/mc^2$, and $\varepsilon(n_h/n_c)(v_h/c) = \eta a_0^2/2$. Thus, the characteristic hot electron density reads as $n_h/n_c = \eta a_0^2(\varepsilon + 1)/2\varepsilon\sqrt{2\varepsilon + \varepsilon^2}$.

In our experiment, $\eta \sim 20\%$ in agreement with [55, 56], which gives the following estimate of $n_h \sim 0.7n_c$ to be used in the calculation of λ_{Dh} included under the logarithm in equation (9). Weak logarithmic dependence on η makes it possible to estimate ε_m with reasonable accuracy even with some uncertainty in η , i.e. $\varepsilon_m \simeq 0.5$ MeV. Note that the rather low

TNSA energy is a consequence of the short duration of the laser pulse, $\tau/\tau_0 \approx 0.5$, which differs from the standard TNSA situation where $\tau > \tau_0$.

It is very likely that the significantly high proton energy measured FWD (see figure 3(a)) indicates the decisive contribution of the Coulomb explosion of the front-side charged cavity, which accelerates ions in both the BWD and FWD directions. Such a scenario can explain the higher energy of protons accelerated FWD due to possible two-step acceleration: protons first accelerate from a cavity and then further accelerate by TNSA. A specialised experiment, for example, with a preliminary cleaning of the backside contaminant, would help to bring complete clarity to this issue.

5.2. 0° laser incidence on the target

At normal laser incidence on the target, $v \times B$ heating dominates the energy transfer process over Brunel's absorption. For our moderate laser intensity of $a_0 \sim 2$, and very short pulse duration, the generation of weakly relativistic hot electrons ($v < c$) at the step-like plasma–vacuum interface prevents effective electron heating. The temporally Gaussian rising edge of the laser pulse creates insufficient electron pre-plasma, and the electrons oscillate along the target surface with slight dominance in the FWD direction. This leads to a very small field amplitude on the target surface, in proportion to the ratio of the skin depth and laser wavelength $\sim \gamma^{1/2} \omega_{L0}/\omega_{ep}$ (where ω_{L0} and ω_{ep} are the laser field and electron plasma frequencies, respectively, and $\gamma = \sqrt{1 + a_0^2/2}$ is the relativistic parameter). As a result, the measured proton energy is half of that compared to 45° laser incidence on the target (figures 3(a) and 4(a)). At oblique laser incidence, the absorption is relevant to the p -component of a laser field, and its overlapping with short pre-plasma increases with the angle of incidence (θ) as $L_{pp}/\cos\theta$. Therefore, one should expect an enhancement of proton acceleration with the increasing θ until almost grazing incidence. This will require further experimental verification for angles $\theta > 45^\circ$.

6. Summary

To summarise, ion acceleration experiments were carried out with few-cycle relativistic laser pulses at intensities of about 10^{19} W cm $^{-2}$ and very high temporal contrast. The measurements of energies of ions accelerated from different target materials with different electron and hydrogen densities (C, DLC, formvar, and Al foil targets) and thicknesses ranging from 5 nm to 9 μ m at laser incidence angles of 0° and 45° to the target normal showed a weak dependence on the target thickness. The measured maximum energy of the protons was ~ 1.4 MeV accelerated laser propagation direction and ~ 1.2 MeV in the opposite direction from the formvar target. From the measured number of particles, the spectral energy content of the proton beam was derived, showing a slowly decaying plateau over a wide energy range for FWD accelerated protons at a 45° angle of laser incidence. A conservative estimate of the laser energy conversion efficiency to protons

showed a clear maximum dependence on the target thickness, reaching the highest value of $\sim 1.4\%$ at a 51 nm thick Al target. The existence of an optimum thickness was explained by the proper match of the foil target thickness to the laser pulse parameters. For an Al target, the ion acceleration efficiency drops sharply for thinner targets compared to the efficiency at the optimal thickness of 50 nm, when foil destruction is likely to begin (for example, at 20 nm, the acceleration efficiency decreases by a factor of five) before the femtosecond laser pulses arrive at the target. Indeed, the selection of a target suitable for certain laser parameters is very promising for increasing the interaction efficiency. The experimental results are in reasonable agreement with theoretical estimates, where proton acceleration from the target front side in the BWD direction is well explained by the Coulomb explosion of a charged cavity formed in a tiny pre-plasma, while FWD proton acceleration is likely to be a two-step process, as the protons first accelerate from a front-side cavity and then further accelerate by backside TNSA.

As an outlook, the measured characteristics of FWD accelerated protons demonstrate that the use of CD instead of CH would make it possible to accelerate deuterons to energies required for fusion neutron production from, e.g. the same CD-catcher. Once the target allows for the use of the kHz repetition rate SYLOS laser at ELI-ALPS, it would be a prototype for a 2.45 MeV neutron source. Additionally, the implantation of protons with an energy of ~ 1 MeV generated by a high repetition rate laser can also be used in semiconductor technology as a new technique to obtain free-standing semiconductor films with thicknesses in the range of 10–20 μ m [57].

Data availability statement

All data that support the findings of this study are included within the article (and any supplementary files).

Acknowledgments

The authors are grateful for the fruitful discussions with Christos Kamperidis, Subhendu Kahaly, Martin Matys, Petr Valenta, Georg Korn, Sergei Bulanov, and Zsolt Fülöp. The authors are indebted to Arnold Farkas, Karoly Mogyorósi, Arpad Mohacsi, Rita Szabó, and Bence Kis for their technical help in the experiments. The project has been supported by the Hungarian Ministry of Technology and Innovation (Contract No. IFHÁT/1039-4/2019-ITM_SZERZ), the Hungarian National Research, Development, and Innovation Office through the National Laboratory program (Contract Nos. NKFIH-877-2/2020 and NKFIH-476-4/2021), and by the Ministry of Education, Youth and Sports of the Czech Republic through the project 'Advanced Research Using High-Intensity Laser-Produced Photons and Particles' (CZ.02.1.010.00.016_0190000789). The ELI-ALPS project is supported by the Hungarian Government and the European Regional Development Fund (Contract No. GINOP-2.3.6-15-2015-00001). V Yu B acknowledges support from the Ministry

of Science and Higher Education of the Russian Federation (under the agreement No. 075-15-2021-1361).

ORCID iDs

Sargis Ter-Avetisyan  <https://orcid.org/0000-0002-6162-0794>

Valery Yu Bychenkov  <https://orcid.org/0000-0001-9624-3813>

Sudipta Mondal  <https://orcid.org/0000-0002-1789-9433>

Daniel Papp  <https://orcid.org/0000-0002-7954-3686>

Zsolt Léczi  <https://orcid.org/0000-0001-5968-8012>

Szabolcs Tóth  <https://orcid.org/0000-0002-8516-3962>

References

- [1] Wagner F *et al* 2016 *Phys. Rev. Lett.* **116** 205002
- [2] Danson C, Hillier D, Hopps N and Neely D 2015 *High Power Laser Sci. Eng.* **3** e3
- [3] Borghesi M *et al* 2008 *Plasma Phys. Control. Fusion* **50** 124040
- [4] Steinke S *et al* 2010 *Laser Part. Beams* **28** 215
- [5] Macchi A, Borghesi M and Passoni M 2013 *Rev. Mod. Phys.* **85** 751
- [6] Green J S *et al* 2014 *Appl. Phys. Lett.* **104** 214101
- [7] Scullion C *et al* 2017 *Phys. Rev. Lett.* **119** 054801
- [8] Snavely R A *et al* 2000 *Phys. Rev. Lett.* **85** 2945
- [9] D'Humieres E, Lefebvre E, Gremillet L and Malka V 2005 *Phys. Plasma* **12** 062704
- [10] Esirkepov T Z, Yamagiwa M and Tajima T 2006 *Phys. Rev. Lett.* **96** 105001
- [11] Bulanov S S *et al* 2008 *Phys. Rev. E* **78** 026412
- [12] Yan X Q, Tajima T, Hegelich B M, Yin L and Habs D 2010 *Appl. Phys. B* **98** 711
- [13] d'Humieres E, Brantov A, Yu Bychenkov V and Tikhonchuk V T 2013 *Phys. Plasmas* **20** 023103
- [14] Borghesi M *et al* 2002 *Phys. Plasmas* **9** 2214
- [15] Kar S *et al* 2016 *New J. Phys.* **18** 053002
- [16] Pelka A *et al* 2010 *Phys. Rev. Lett.* **105** 265701
- [17] Kraft S D *et al* 2010 *New J. Phys.* **12** 085003
- [18] Raschke S, Spickermann S, Toncian T, Swantusch M, Boeker J, Giesen U, Iliakis G, Willi O and Boege F 2016 *Sci. Rep.* **6** 32441
- [19] Ziegler T *et al* 2021 *Sci. Rep.* **11** 7338
- [20] Permogorov A, Cantono G, Guenot D, Persson A and Wahlström C G 2022 *Sci. Rep.* **12** 3031
- [21] Bin J *et al* 2022 *Sci. Rep.* **12** 1484
- [22] Cirrone G A P *et al* 2020 *Front. Phys.* **8** 564907
- [23] Kroll F *et al* 2022 *Nat. Phys.* **18** 316
- [24] Toth S *et al* 2020 *J. Phys. Photon.* **2** 045003
- [25] Tomkus V, Girdauskas V, Dudutis J, Gečys P, Stankevič V and Račiukaitis G 2018 *Opt. Express* **26** 27966
- [26] Morrison G J T *et al* 2019 *High Power Laser Sci. Eng.* **7** e50
- [27] Rovige L *et al* 2020 *Phys. Rev. Acc. Beams* **23** 093401
- [28] Morrison J T, Feister S, Frische K D, Austin D R, Ngirmang G K, Murphy N R, Orban C, Chowdhury E A and Roquemore W M 2018 *New J. Phys.* **20** 022001
- [29] MultiScan 3D project *Laser-plasma based source 3D Tomography for cargo inspection* (available at: <https://cordis.europa.eu/project/id/101020100>)
- [30] Gesellschaft für Schwerionenforschung (GSI) Laser ion generation, handling and transport (LIGHT) at GSI (available at: www.gsi.de/work/forschung/appamml/plasmaphysikphelix/experimente/light.htm)
- [31] Fritzier S, Malka V, Grillon G, Rousseau J P, Burgy F, Lefebvre E, D'humieres E, McKenna P and Ledingham K W D 2003 *Appl. Phys. Lett.* **83** 3039
- [32] Lefebvre E 2006 *J. Appl. Phys.* **100** 113308
- [33] Veltcheva M, Borot A, Thauray C, Malvache A, Lefebvre E, Flacco A, Lopez-Martens R and Malka V 2012 *Phys. Rev. Lett.* **108** 075004
- [34] Levy D, Andriyash I A, Haessler S, Kaur J, Ouillé M, Flacco A, Kroupp E, Malka V and Lopez-Martens R 2022 *Phys. Rev. Acc. Beams* **25** 093402
- [35] Singh P K, Kakolee K F, Jeong T W and Ter-Avetisyan S 2016 *Nucl. Instrum. Methods A* **829** 363
- [36] Varmazyar P *et al* 2022 *Rev. Sci. Instrum.* **93** 073301
- [37] Ceccotti T, Lévy A, Popescu H, Réau F, D'Oliveira P, Monot P, Geindre J P, Lefebvre E and Martin P 1977 *Phys. Rev. Lett.* **39** 284
- [38] Singh P K, Varmazyar P, Nagy B, Son J-G, Ter-Avetisyan S and Osvay K 2022 *Sci. Rep.* **12** 8100
- [39] Ter-Avetisyan S, Schnürer M, Nickles P V, Sandner W, Nakamura T and Mima K 2009 *Phys. Plasmas* **16** 043108
- [40] Ter-Avetisyan S, Romagnani L, Borghesi M, Schnürer M and Nickles P V 2010 *Nucl. Instrum. Methods A* **623** 709
- [41] Dollar F *et al* 2011 *Phys. Rev. Lett.* **107** 065003
- [42] Dollar F *et al* 2012 *Phys. Rev. Lett.* **108** 175005
- [43] Brantov A V, Govras E A and Yu Bychenkov V 2015 *Phys. Rev. ST* **18** 021301
- [44] Sentoku Y, Bychenkov V Y, Flippo K, Maksimchuk A, Mima K, Mourou G, Sheng Z M and Umstadter D 2002 *Appl. Phys. B* **74** 207
- [45] Mordovanakis A G *et al* 2009 *Phys. Rev. Lett.* **103** 235001
- [46] Batani D *et al* 2010 *New J. Phys.* **12** 045018
- [47] Lecz Z, Budai J, Andreev A and Ter-Avetisyan S 2020 *Phys. Plasmas* **27** 013105
- [48] Forslund D W, Kindel J M and Lee K 1977 *Phys. Rev. Lett.* **39** 284
- [49] Brunel F 1987 *Phys. Rev. Lett.* **59** 52
- [50] Kruer W L and Estabrook K 1985 *Phys. Fluids* **28** 430
- [51] Yogo A *et al* 2016 *Plasma Phys. Control. Fusion* **58** 025003
- [52] Yu Bychenkov V *et al* 2017 *Phys. Plasmas* **24** 010704
- [53] Mora P 2003 *Phys. Rev. Lett.* **90** 185002
- [54] Bychenkov V Y, Novikov V N, Batani D, Tikhonchuk V T and Bochkarev S G 2004 *Phys. Plasmas* **11** 3242
- [55] Fedeli L, Formenti A, Cialfi L, Pazzaglia A and Passoni M 2018 *Sci. Rep.* **8** 3834
- [56] Cialfi L, Fedeli L and Passoni M 2016 *Phys. Rev. E* **94** 053201
- [57] Huang K *et al* 2018 *Appl. Phys. A* **124** 118